

DOI:10.1002/ejic.201500059

Electronic Fine-Tuning of Oxygen Atom Transfer Reactivity of *cis*-Dioxomolybdenum(VI) Complexes with Thiosemicarbazone Ligands

Aurélien Ducrot,^[a] Bethany Scattergood,^[a] Ben Coulson,^[a] Robin N. Perutz,^[a] and Anne-K. Duhme-Klair^{*[a]}

Keywords: Enzyme models / Metalloenzymes / Molybdenum / Oxygen atom transfer / Ligand effects

A series of six *cis*-dioxomolybdenum(VI) complexes with thiosemicarbazone ligands was synthesized and characterized. The ligands were obtained by reacting ethyl thiosemicarbazide with salicylaldehydes substituted with a selection of electron-withdrawing and electron-donating groups. The crystal structures, IR, NMR spectroscopic data and oxygen atom transfer activities of the complexes revealed that the electronic effects of the substituents located in the *para*-position of the phenolate donor are transmitted through to the molybdenum center, as reflected by linear

relationships between Hammett constants and key properties of the complexes, including the molybdenum–phenolate bond lengths and the coordination shift of the imine proton resonance. Compared with the unsubstituted catalyst, electron-withdrawing substituents increase the rate of oxygen atom transfer from dimethyl sulfoxide to triphenylphosphine, whereas electron-donating groups have the opposite effect. The highest rate enhancement was achieved through the introduction of a strongly electron-withdrawing NO₂ substituent in the *p*-position of the phenolate donor.

Introduction

Nature uses the ability of molybdenum to switch between oxidation states (VI) and (IV) to catalyze oxygen atom transfer (OAT) reactions.^[1] In molybdoenzymes, the two electrons that are released during substrate oxidation are rapidly transferred to spatially separated one-electron transfer components, such as heme and/or Fe–S clusters. Finally, the reducing equivalents generated are handed over to a terminal electron acceptor.

A range of structurally diverse dioxomolybdenum(VI) complexes have been developed with the aim of catalyzing biomimetic and industrially relevant OAT reactions.^[2–6] Whereas bidentate dithiolene ligands model the S,S donor set found in the molybdopterin cofactor of the enzymes,^[7,8] bidentate ligands with N,S, N,N and N,O donor have also been found to catalyze OAT. Examples include pyridine thiolates,^[9] iminopyrrolato,^[10,11] diketiminate (NacNac),^[12] and β -ketiminato^[13] ligands. In addition, dioxo-molybdenum complexes with ligands of higher denticity and mixed donor sets have shown promise (Figure 1). Commonly studied tridentate ligands include facially coordinating hydrotris(pyrazolyl)borates (e.g., Tp*, **1**^[14–16]) and meridionally coordinating Schiff base derivatives (e.g., ssp, **2**^[17] and

tsc, **3**^[18,19]). Whereas tridentate ligands can occupy only three of the four available coordination sites on the *cis*-MoO₂ center, tetradentate ligands, including tripodal (N3O, **4**^[20]) or linear (salan^[21,22]) ligands (**5**) form coordinatively saturated complexes.

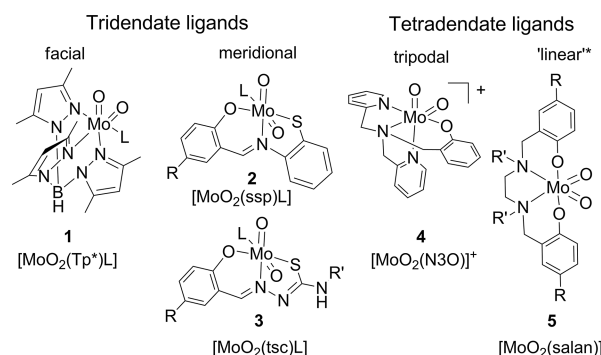


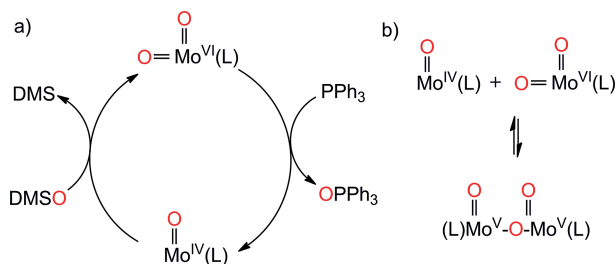
Figure 1. Schematic representation of the structures of selected biomimetic *cis*-dioxomolybdenum(VI) complexes with multidentate ligands (L = solvent molecule, * “linear” indicates donor atom connectivity rather than 3D structure).

To assess the catalytic activity of functional model complexes, the thermodynamically favorable OAT from sulfides to tertiary phosphines is often used as a benchmark reaction. Biomimetic model complexes, however, tend not to have additional redox centers incorporated, as found in the molybdoenzymes, and hence both the oxidative and reductive half-reaction take place at the molybdenum center (Scheme 1).^[23] The catalytic activity of these complexes is

[a] Department of Chemistry, University of York, Heslington, York, YO10 5DD, United Kingdom
E-mail: anne.duhme-klair@york.ac.uk
http://www.york.ac.uk/chemistry/staff/academic/d-g/a-kduhme-klair/

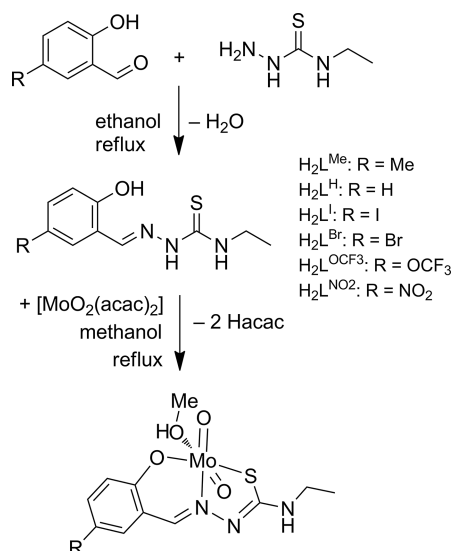
Supporting information for this article is available on the WWW under <http://dx.doi.org/10.1002/ejic.201500059>.

therefore often limited by slow kinetics due to charge build-up at the molybdenum center and the formation of inactive Mo^V dimers as a result of the comproportionation of Mo^{IV} and Mo^{VI} (Scheme 1).



Scheme 1. (a) Simplified catalytic cycle for the biomimetic oxygen atom transfer (OAT) from dimethyl sulfoxide (DMSO) to triphenylphosphine (PPh_3) to give dimethyl sulfide (DMS) and triphenylphosphine oxide (OPPh_3); (b) Comproportionation reaction leading to the formation of a dinuclear, oxo-bridged Mo^V complex.

In this context, we are interested in the development of chelate ligands that allow the electronic properties of their donor atoms to be tuned so as to facilitate OAT. Thiosemicarbazone ligands attract much attention because they are straightforward to synthesize and have scope for structural diversity. The research area has recently been reviewed.^[24] In particular, thiosemicarbazones derived from salicylaldehydes allow a systematic investigation of the effect of electron-withdrawing groups (EWGs) or electron-donating groups (EDGs) on the electronic properties of a coordinated molybdenum center. It was found that these electronic trends are reflected in the spectroscopic properties of the molybdenum complexes formed,^[18,25] and in their catalytic,^[26] biological,^[27,28] and pharmacological properties.^[29,30]



Scheme 2. Synthesis of six thiosemicarbazone ligands and their *cis*-dioxo Mo^{VI} complexes (hacac = acetylacetonate).

Here we present the synthesis, characterization and catalytic OAT activity of a series of *cis*-dioxomolybdenum(VI) complexes with structurally related tridentate thiosemicarbazone ligands (Scheme 2). The complexes feature a selection of EWGs and EDGs located in the *para*-position of the phenolate donor that allow for a Hammett analysis of their OAT reactivity.

Results and Discussion

Compound Design, Synthesis, and Characterization

To allow for a systematic Hammett analysis of the effects of a *p*-aryl substituent on the electron density of the phenolate donor and hence the molybdenum center, the following electron-donating and electron-withdrawing groups were chosen (corresponding Hammett constants^[31] σ_p given in parenthesis): Me (−0.17), H (0), I (0.18), Br (0.23), OCF_3 (0.35), and NO_2 (0.78). The rather unusual trifluoromethoxy group was included in the series because of its increasing use in the development of bioactive molecules.^[32] For ligands adjacent in the series (i.e., with similar Hammett parameters), the properties discussed below are not always significantly different if experimental errors are taken into account. Therefore, discussions are based on observed trends rather than on quantitative differences between compounds that have similar Hammett constants.

Six thiosemicarbazone ligands were prepared by heating ethanolic solutions of the respective *para*-substituted 2-hydroxy salicylaldehyde to reflux with an equimolar amount of ethyl thiosemicarbazide (Scheme 2). The thiosemicarbazones formed were isolated following partial removal of the solvent. Evidence for the formation of the imine bond was provided by the appearance of a singlet resonance for the imine proton at 8.32–8.38 ppm and loss of the resonance due to the aldehyde proton in the ^1H NMR spectra ($[\text{D}_6]\text{DMSO}$). Corroborating evidence was obtained by ^{13}C NMR and FTIR spectroscopy.

Subsequently, the six ligands H_2L^R were coordinated to a *cis*-dioxo Mo^{VI} center and the resulting $[\text{MoO}_2(\text{L}^R)\text{MeOH}]$ complexes were isolated and characterized. Evidence of complex formation was seen in the ^1H NMR spectra with the imine proton resonance shifting downfield by 0.14–0.36 ppm ($[\text{D}_6]\text{DMSO}$) and loss of the OH and one of the NH resonances due to deprotonation upon coordination. IR spectroscopic data also confirmed complex formation, with $\nu(\text{C}=\text{N})$ shifting to lower frequencies upon molybdenum binding. Good quality mass spectra of the complexes with well-resolved isotope patterns could be obtained by using liquid injection field desorption/ionization (LIFDI).^[33]

Whereas the syntheses of H_2L^H , $\text{H}_2\text{L}^{\text{Me}}$,^[29] $\text{H}_2\text{L}^{\text{Br}}$,^[34] $[\text{MoO}_2(\text{L}^{\text{Me}})\text{MeOH}]$,^[29] and $[\text{MoO}_2(\text{L}^{\text{Br}})\text{MeOH}]$ ^[34] have been reported previously, the availability of characterization data varies depending on the selection of techniques and conditions used in each case. Hence, for completion and for

comparison purposes, full characterization data of the six ligands and complexes were obtained and are provided in the Experimental Section. LIFDI and IR spectra can be found in the Supporting Information.

X-ray Structures

Diffraction-quality crystals of all six $[\text{MoO}_2(\text{L}^{\text{R}})\text{MeOH}]$ complexes were obtained and their crystal structures were determined. Selected bond lengths and angles and crystallographic data are summarized in Tables 1 and 2, respectively. The crystal structures confirmed that the thiosemicar-

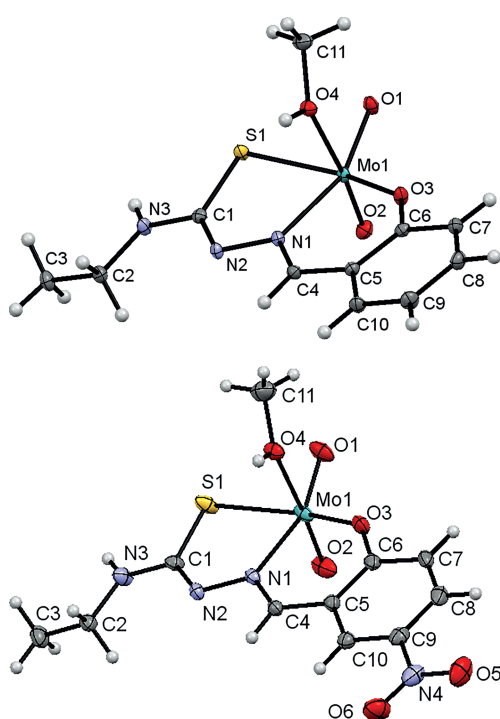


Figure 2. ORTEP plots (50% probability ellipsoids) of the molecular structure of $[\text{MoO}_2(\text{L}^{\text{H}})\text{MeOH}]$ (top) and $[\text{MoO}_2(\text{L}^{\text{NO}_2})\text{MeOH}]$ (bottom); only one enantiomer is shown; configuration index OC-6-24, chirality symbol C.

azones act as meridionally coordinating dianionic ligands with the sulfur, oxygen, and imine nitrogen donors contributing to the coordination sphere. In addition, two oxo ligands and a molecule of MeOH coordinate to the Mo^{VI} centers to form distorted octahedral complexes with configuration index OC-6-24.^[35,36] Figure 2 shows the molecular structures of the parent complex $[\text{MoO}_2(\text{L}^{\text{H}})\text{MeOH}]$ and the most active catalyst of the series, $[\text{MoO}_2(\text{L}^{\text{NO}_2})\text{MeOH}]$, as representative examples; the other ORTEP plots are shown in the Supplementary Information. Selected bond lengths and angles (Table 1) agree well with those reported for similar *cis*-dioxo Mo^{VI} complexes.^[18,27,28,37–40]

The crystals consist of racemic mixtures of OC-6-24-*A*- and OC-6-24-*C*-configured^[35,36] enantiomers. The complexes crystallize in centrosymmetric space groups $P2_1/c$ $\{[\text{MoO}_2(\text{L}^{\text{Me}})\text{MeOH}], [\text{MoO}_2(\text{L}^{\text{NO}_2})\text{MeOH}]\}$ and $P\bar{1}$ $\{[\text{MoO}_2(\text{L}^{\text{H}})\text{MeOH}], [\text{MoO}_2(\text{L}^{\text{Br}})\text{MeOH}], [\text{MoO}_2(\text{L}^{\text{I}})\text{MeOH}], [\text{MoO}_2(\text{L}^{\text{OCF}_3})\text{MeOH}]\}$, in which the asymmetric unit contains one of the enantiomers and the second enantiomer is symmetry generated through rotoinversion axes and/or inversion centers, respectively.

As a consequence of the meridionally coordinating O,N,S ligand, the two oxo ligands on the Mo^{VI} centers are inequivalent: one is positioned *trans* to the N donor, whereas the second is coordinated *trans* to the O donor of methanol. This may be relevant because it was recently reported that a *trans*-effect that weakens the Mo–oxo bond of the catalytically active group can give rise to enhanced OAT activity.^[41] In the $[\text{MoO}_2(\text{L}^{\text{R}})\text{MeOH}]$ complexes, the Mo–O1 bonds *trans* to the imine N donor tend to be slightly longer than the Mo–O2 bonds in the *trans*-position of the weakly coordinated methanol.

The phenolate donor (O3) is the donor atom that is closest to the remote substituent R; therefore it is the one that is most likely to be affected by differences in their electronic properties. The Hammett plot, shown in Figure 3, correlates the electron-withdrawing/donating properties of the substituent R in the *p*-position to the phenolate substituent of the aromatic ring with the Mo–O3 bond lengths. EWGs, in particular the strongly electron-withdrawing NO_2 group, lower the electron density of the aromatic ring, which, in turn, reduces the electron density on the phen-

Table 1. Selected bond lengths and angles for $[\text{MoO}_2(\text{L}^{\text{R}})\text{MeOH}]$, with R = Me, H, I, Br, OCF_3 , and NO_2 .

Bond [Å]	$[\text{MoO}_2(\text{L}^{\text{Me}})\text{MeOH}]$	$[\text{MoO}_2(\text{L}^{\text{H}})\text{MeOH}]$	$[\text{MoO}_2(\text{L}^{\text{I}})\text{MeOH}]$	$[\text{MoO}_2(\text{L}^{\text{Br}})\text{MeOH}]$	$[\text{MoO}_2(\text{L}^{\text{OCF}_3})\text{MeOH}]$	$[\text{MoO}_2(\text{L}^{\text{NO}_2})\text{MeOH}]$
Mo–O1	1.7118(12)	1.7042(13)	1.703(2)	1.7025(12)	1.7045(12)	1.7076(16)
Mo–O2	1.6941(13)	1.7022(12)	1.692(2)	1.6997(13)	1.6942(14)	1.6964(17)
Mo–O3	1.9304(12)	1.9327(13)	1.932(2)	1.9340(12)	1.9371(13)	1.9488(15)
Mo–O4	2.3503(12)	2.3471(12)	2.313(2)	2.3058(12)	2.3011(14)	2.3015(15)
Mo–S1	2.4224(4)	2.4147(5)	2.4105(8)	2.4148(5)	2.4325(5)	2.4199(6)
Mo–N1	2.2755(13)	2.2803(14)	2.296(2)	2.2908(14)	2.2880(14)	2.2949(16)
C1–S1	1.7493(16)	1.7489(17)	1.753(3)	1.7493(17)	1.7379(17)	1.746(2)
Angle [°]						
O1–Mo–O2	105.61(6)	105.46(6)	105.67(11)	105.57(6)	106.19(7)	105.34(8)
O1–Mo–N1	158.73(5)	156.36(5)	159.11(10)	159.16(6)	159.41(6)	159.90(7)
N1–Mo–S1	75.78(3)	76.20(4)	76.29(7)	76.34(4)	76.21(4)	75.72(4)
O3–Mo–N1	83.38(5)	82.37(5)	82.85(9)	82.77(5)	82.35(5)	82.26(6)

Table 2. Crystallographic data for $[\text{MoO}_2(\text{L}^{\text{R}})\text{MeOH}]$, with R = Me, H, I, Br, OCF_3 , and NO_2 .

	$[\text{MoO}_2(\text{L}^{\text{H}})(\text{MeOH})]$	$[\text{MoO}_2(\text{L}^{\text{Me}})(\text{MeOH})]$	$[\text{MoO}_2(\text{L}^{\text{Br}})(\text{MeOH})]$
CCDC deposition number	1042299	104301	1042300
Empirical formula	$\text{C}_{11}\text{H}_{15}\text{MoN}_3\text{O}_4\text{S}$	$\text{C}_{12}\text{H}_{17}\text{MoN}_3\text{O}_4\text{S}$	$\text{C}_{11}\text{H}_{14}\text{BrMoN}_3\text{O}_4\text{S} + 1 (\text{CH}_4\text{O})$
Molecular weight	381.26	395.28	492.20
Crystal system	triclinic	monoclinic	triclinic
Space group	$P\bar{1}$	$P2_1/c$	$P\bar{1}$
a [Å]	7.4031(5)	7.55956(10)	7.5586(5)
b [Å]	9.4211(6)	18.9597(2)	9.4460(5)
c [Å]	10.8189(7)	10.72806(14)	12.3311(8)
α [°]	87.104(5)	90	78.820(5)
β [°]	72.698(6)	108.7103(15)	75.754(5)
γ [°]	72.365(6)	90	85.855(5)
Volume [Å ³]	685.92(8)	1456.36(3)	836.88(9)
Z	2	4	2
$\rho_{\text{calcd.}}$ [g/cm ³]	1.846	1.803	1.953
M [mm ⁻¹]	1.125	1.063	3.322
$F(000)$	384.0	800.0	488.0
2 θ range for data collection [°]	5.886 to 64.584	7.132 to 64.364	6.808 to 64.338
Index ranges	$-10 \leq h \leq 11$, $-13 \leq k \leq 14$, $-16 \leq l \leq 15$	$-11 \leq h \leq 10$, $-27 \leq k \leq 26$, $-16 \leq l \leq 15$	$-11 \leq h \leq 10$, $-13 \leq k \leq 13$, $-18 \leq l \leq 17$
Reflections collected	12447	13617	15598
Independent reflections	4459	4717	5410
Data/restraints/parameters	$[R_{\text{int}} = 0.0384, R_{\text{sigma}} = 0.0508]$ 4459/0/191	$[R_{\text{int}} = 0.0258, R_{\text{sigma}} = 0.0308]$ 4717/0/201	$[R_{\text{int}} = 0.0251, R_{\text{sigma}} = 0.0297]$ 5410/0/222
Goodness-of-fit on F^2	1.069	1.061	1.038
Final R indexes [$I \geq 2\sigma(I)$]	$R_1 = 0.0271, wR_2 = 0.0567$	$R_1 = 0.0250, wR_2 = 0.0549$	$R_1 = 0.0233, wR_2 = 0.0502$
Final R indexes [all data]	$R_1 = 0.0318, wR_2 = 0.0594$	$R_1 = 0.0297, wR_2 = 0.0578$	$R_1 = 0.0285, wR_2 = 0.0524$
Largest diff. peak/hole [e Å ⁻³]	0.69/−0.78	0.48/−0.67	0.54/−0.63
	$[\text{MoO}_2(\text{L}^{\text{I}})(\text{MeOH})]$	$[\text{MoO}_2(\text{L}^{\text{OCF}_3})(\text{MeOH})]$	$[\text{MoO}_2(\text{L}^{\text{NO}_2})(\text{MeOH})]$
CCDC deposition number	104303	104304	1042302
Empirical formula	$\text{C}_{11}\text{H}_{14}\text{IMoN}_3\text{O}_4\text{S} + 1 (\text{CH}_4\text{O})$	$\text{C}_{12}\text{H}_{14}\text{F}_3\text{MoN}_3\text{O}_5\text{S}$	$\text{C}_{11}\text{H}_{14}\text{MoN}_4\text{O}_6\text{S} + 1.5 (\text{CH}_4\text{O})$
Molecular weight	539.19	465.26	474.32
Crystal system	triclinic	triclinic	monoclinic
Space group	$P\bar{1}$	$P\bar{1}$	$P2_1/c$
a [Å]	7.6024(5)	7.9658(4)	7.61510(14)
b [Å]	9.5206(6)	9.4849(3)	13.4754(2)
c [Å]	12.4608(9)	10.7998(4)	17.8271(3)
α [°]	77.984(6)	93.431(3)	90
β [°]	75.848(6)	91.398(3)	101.3340(17)
γ [°]	85.882(5)	91.144(3)	90
Volume [Å ³]	855.17(10)	814.09(5)	1793.68(5)
Z	2	2	4
$\rho_{\text{calcd.}}$ [g/cm ³]	2.094	1.898	1.756
μ [mm ⁻¹]	2.721	0.996	0.894
$F(000)$	524.0	464.0	964.0
2 θ range for data collection [°]	6.752 to 64.406	6.616 to 64.326	7.026 to 64.342
Index ranges	$-11 \leq h \leq 11$, $-13 \leq k \leq 12$, $-16 \leq l \leq 18$	$-11 \leq h \leq 11$, $-13 \leq k \leq 13$, $-16 \leq l \leq 15$	$-10 \leq h \leq 11$, $-19 \leq k \leq 19$, $-26 \leq l \leq 26$
Reflections collected	9123	15061	22461
Independent reflections	5387	5261	5876
Data/restraints/parameters	$[R_{\text{int}} = 0.0360, R_{\text{sigma}} = 0.0559]$ 5387/0/220	$[R_{\text{int}} = 0.0370, R_{\text{sigma}} = 0.0385]$ 5261/0/233	$[R_{\text{int}} = 0.0317, R_{\text{sigma}} = 0.0287]$ 5876/0/267
Goodness-of-fit on F^2	1.066	1.045	1.053
Final R indexes [$I \geq 2\sigma(I)$]	$R_1 = 0.0367, wR_2 = 0.0856$	$R_1 = 0.0277, wR_2 = 0.0607$	$R_1 = 0.0323, wR_2 = 0.0795$
Final R indexes [all data]	$R_1 = 0.0461, wR_2 = 0.0962$	$R_1 = 0.0334, wR_2 = 0.0637$	$R_1 = 0.0417, wR_2 = 0.0853$
Largest diff. peak/hole [e Å ⁻³]	1.65/−1.37	0.70/−0.72	1.12/−0.78

olate donor in the p -position. Hence, the donor strength of the phenolate group is reduced and the Mo–O3 bond becomes longer and weaker. As expected, the electron-donating methyl group has the opposite effect. However, this

trend is not reflected by the other molybdenum donor bonds, either because they are too far away from the remote substituent or because of packing effects that may mask any electronic effects.

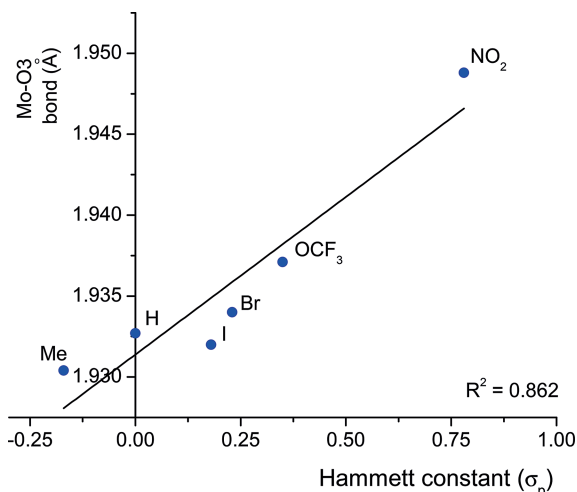


Figure 3. Plot of the Hammett constant σ_p vs. Mo–O3 bond lengths [Å].

IR and NMR Spectroscopic Investigations

Selected IR spectroscopic data and ^1H NMR chemical shifts are summarized in Table 3. To assess whether or not the electronic properties of the remote substituent R are transmitted through to the *cis*-dioxomolybdenum core, we examined the $\nu(\text{MoO}_2)$ stretching frequencies. As can be seen from the Hammett plot in Figure 4, there is an approximate correlation between the Hammett constant for the remote substituent R and the position of the IR band due to the asymmetric $\nu(\text{MoO}_2)$ stretching vibration for five of the six complexes (R = Me, H, I, Br, and OCF_3). A similar observation was reported by Krebs et al. for *cis*-dioxomolybdenum complexes derived from (triphenylmethyl)-thiosemicarbazones.^[18] EWGs, such as CF_3 , result in a band at higher frequency, whereas net EDGs, such as Me, result in a band at lower frequency. The asymmetric $\nu(\text{MoO}_2)$ stretching frequency obtained for the nitro-substituted compound is lower than expected and does not fit the predicted trend. Similarly, the symmetric stretching frequencies of the six complexes do not fit the trend, potentially due to crystal-packing effects in the solid state.

Given that the effects of the electron-donating or electron-withdrawing aromatic substituents R observed in the solid state cannot be easily deconvoluted from crystal-packing effects, additional information was obtained from the NMR spectra measured in solution ($[\text{D}_6]\text{DMSO}$).

To determine the electronic substituent effects on the coordinated thiosemicarbazone ligands, the coordination shift, defined as $\Delta\delta = \delta_{\text{coordinated ligand}} - \delta_{\text{free ligand}}$, was plotted against the Hammett constant (Figure 5). This relative approach eliminates the intrinsic effect that a particular substituent has on the chemical shift of a resonance. Hence, the coordination shift reflects the effect of the substituents on the metal–ligand interactions.

An examination of the Hammett plot shown in Figure 5 indicates that there is a linear relationship between the coordination shift of the imine proton and the Hammett constant σ_p . Consequently, the remote substituent in the *para*-

Table 3. Selected ^1H NMR chemical shifts and IR spectroscopic data.

Compounds	^1H NMR		IR	
	δ [ppm]	δ [ppm]	$\tilde{\nu}$ [cm^{-1}]	$\tilde{\nu}$ [cm^{-1}]
	CHN	NH	$\nu(\text{MoO}_2)_{\text{asym.}}$	$\nu(\text{MoO}_2)_{\text{sym.}}$
$\text{H}_2\text{L}^{\text{Me}}$	8.33	8.44	–	–
$[\text{MoO}_2(\text{L}^{\text{Me}})\text{MeOH}]$	8.47	7.49	896	934
$\text{H}_2\text{L}^{\text{H}}$	8.36	8.47	–	–
$[\text{MoO}_2(\text{L}^{\text{H}})\text{MeOH}]$	8.55	7.52	901	930
$\text{H}_2\text{L}^{\text{I}}$	8.27	8.56	–	–
$[\text{MoO}_2(\text{L}^{\text{I}})\text{MeOH}]$	8.50	7.64	906	937
$\text{H}_2\text{L}^{\text{Br}}$	8.29	8.65	–	–
$[\text{MoO}_2(\text{L}^{\text{Br}})\text{MeOH}]$	8.53	7.65	906	942
$\text{H}_2\text{L}^{\text{OCF}_3}$	8.28	8.60	–	–
$[\text{MoO}_2(\text{L}^{\text{OCF}_3})\text{MeOH}]$	8.59	7.69	908	937
$\text{H}_2\text{L}^{\text{NO}_2}$	8.37	8.75	–	–
$[\text{MoO}_2(\text{L}^{\text{NO}_2})\text{MeOH}]$	8.73	7.80	899	941

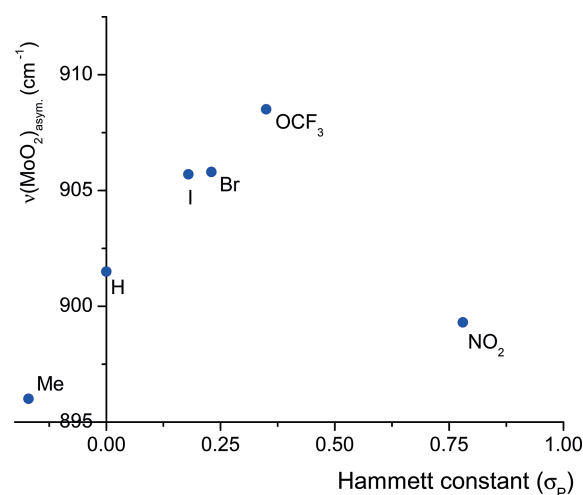


Figure 4. Plot of the Hammett constant σ_p vs. $\nu(\text{MoO}_2)_{\text{asym.}}$ stretching frequency.

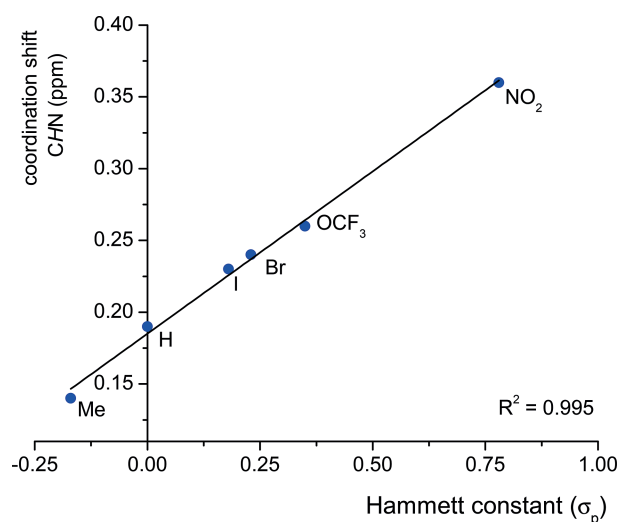


Figure 5. Plot of the coordination shift of the imine proton resonance [ppm] vs. the Hammett constant σ_p .

position of the aromatic ring is likely to influence the bonding between the molybdenum and the ligand through the

donor strength of the imine nitrogen. EWGs lead to more drastic deshielding of the imine proton, whereas the deshielding observed with the electron-donating methyl substituent is less pronounced.

Catalytic Oxygen Atom Transfer Activity

Catalytic oxygen atom transfer (OAT) between triphenylphosphine and dimethyl sulfoxide was investigated at room temperature by ^{31}P NMR spectroscopy using an excess of PPh_3 over catalyst. The decrease of the PPh_3 concentration was monitored over time and the reaction was found to be *pseudo*-first-order with respect to $[\text{PPh}_3]$. The *pseudo*-first-order rate constants (k_{obs}) were determined by plotting $\ln([\text{PPh}_3]_t/[\text{PPh}_3]_0)$ vs. time followed by analysis by linear regression. The results obtained at a catalyst concentration of 5 mM are shown in Figure 6; the corresponding plots for 2, 3.5, 7.5 and 10 mM catalyst concentrations can be found in the Supporting Information. The *pseudo*-first-order rate constants obtained are listed in Table 4. Whereas the k_{obs} values obtained for the Me- and H-substituted catalysts are similar, as are those obtained with I-, Br-, and OCF_3 -substituted catalysts, the NO_2 -substituted catalyst showed significantly higher activity. For $[\text{MoO}_2(\text{L}^{\text{NO}_2})\text{MeOH}]$, the $\ln([\text{PPh}_3]_t/[\text{PPh}_3]_0)$ vs. time graph deviates from linearity at longer reaction times, when the conversion of PPh_3 into OPPh_3 exceeds approximately 50%. This may be caused by catalyst deactivation, for example through formation of oxo-bridged Mo^{V} dimers (Scheme 1), or a shift in rate-determining step (see below).

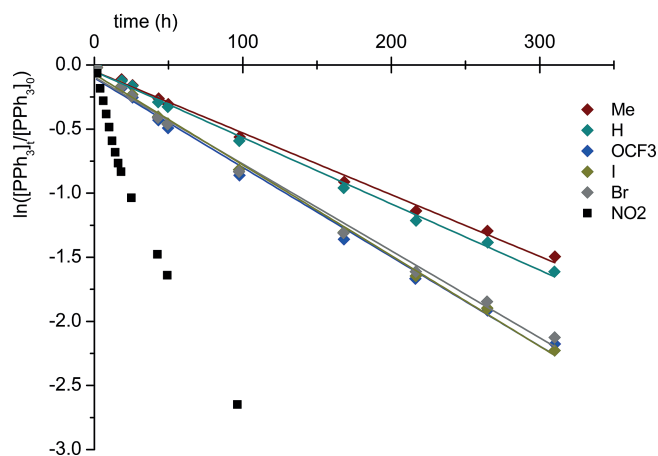


Figure 6. Plot of the decrease in $\ln([\text{PPh}_3]_t/[\text{PPh}_3]_0)$ over time during the OAT reaction between PPh_3 and DMSO ($[\text{PPh}_3]_0 = 127.5 \text{ mM}$ (25.5 equiv.), $[\text{cat}] = 5 \text{ mM}$ (1 equiv.) in 50% $\text{CD}_2\text{Cl}_2/50\%$ $[\text{D}_6]\text{DMSO}$ at room temperature).

The log of the normalized rate constants ($k_{\text{R,obs}}/k_{\text{H,obs}}$ where $k_{\text{R,obs}}$ is the rate obtained with the respective *p*-substituent R, and $k_{\text{H,obs}}$ is the rate obtained with the unsubstituted ligand; 5 mM catalyst concentration) plotted against the Hammett constant σ_p is shown in Figure 7. It is evident that the rate of PPh_3 oxidation, as reflected by growth in k_{obs} with the electron-withdrawing ability of the remote *p*-substituent on the catalyst, is indicative of a build-up of

Table 4. *Pseudo*-first-order rate constants (k_{obs}) and second-order rate constants (k_2) for the OAT reaction between PPh_3 and DMSO at room temperature ($[\text{catalyst}] = 2, 3.5, 5, 7.5, 10 \text{ mM}$, $[\text{PPh}_3] = 127.5 \text{ mM}$, solvent: 50% CD_2Cl_2 , 50% $[\text{D}_6]\text{DMSO}$).

$[\text{MoO}_2(\text{L}^{\text{R}})\text{MeOH}]$						
R =	Me	H	I	Br	OCF_3	$\text{NO}_2^{\text{[a]}}$
$k_{\text{obs}} 10^7 [\text{s}^{-1}]$						
2 mM	5.7(1)	7.2(1)	8.8(1)	9.9(1)	10.0(1)	50(1)
3.5 mM	10.3(2)	12.6(2)	17(1)	15.8(4)	17(1)	90(2)
5 mM	14.5(3)	15.4(3)	21(1)	21(1)	22(1)	135(3)
7.5 mM	20.2(6)	24(1)	24(1)	33(2)	30(1)	200(3)
10 mM	25(1)	29(1)	38(1)	34(1)	38(2)	237(5)
$k_2 10^4 [\text{M}^{-1}\text{s}^{-1}]$	2.4(1)	2.8(1)	3.3(5)	3.2(5)	3.5(1)	24(2)
σ_p	-0.17	0	0.18	0.23	0.35	0.78

[a] Rate based only on the linear part of the graph (up to a reaction time of 18 h).

negative charge during the rate-determining step in the catalytic cycle. This observation is consistent with the generally accepted OAT mechanism involving nucleophilic attack of the phosphine lone pair on a vacant π^* orbital of one of the oxo ligands on the *cis*- $\text{Mo}^{\text{VI}}\text{O}_2$ unit, leading to the formation of the corresponding $\text{Mo}^{\text{IV}}\text{O}$ complex and phosphine oxide via a phosphine oxide-coordinated intermediate.^[42,43] Accordingly, if EWGs decrease the electron density on the $\text{Mo}^{\text{VI}}\text{O}_2$ center, the oxo ligand becomes more susceptible to attack. In addition, if EWGs lower the energy of the transition state by ameliorating negative charge build-up, they give rise to faster reaction rates.

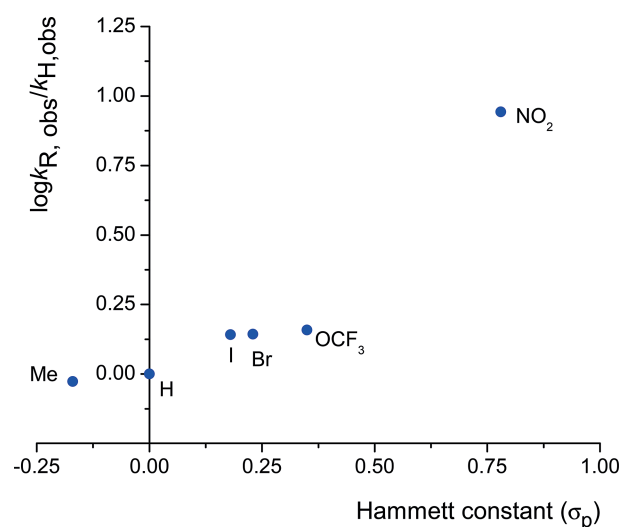


Figure 7. Plot of the relative rate constants $\log k_{\text{R,obs}}/k_{\text{H,obs}}$ vs. the Hammett parameter σ_p for $[\text{cat}] = 5 \text{ mM}$.

Similar observations have previously been made with other ligands, including other tridentate Schiff base ligands, such as those obtained by condensation of substituted salicylaldehydes with *ortho*-aminobenzenethiol,^[17] substituted thiophenolate,^[44] substituted dithiolenes,^[45] and salan-type ligands.^[21,41] A particularly pronounced effect of the NO_2 substituent was also observed by Britovsek and Gibson et al. with dioxomolybdenum complexes with *para*-substituted salan-type ligands.^[21]

To determine the corresponding second-order rate constants, analogous OAT transfer experiments were carried out by using a range of catalyst concentrations (2, 3.5, 5, 7.5, and 10 mM). For all six catalysts, the dependence of k_{obs} on catalyst concentration was found to be linear, indicating that the OAT reaction is also first order in catalyst. Hence, the kinetic data can be interpreted as second order overall [Equation (1), Experimental Section]. From the slopes of the graphs shown in Figure 8, second-order rate constants (k_2), which are independent of catalyst concentration, were obtained (Table 4). The second-order rate constants for the Me-, H-, I-, Br-, and OCF₃-substituted catalysts are similar and increase slightly with increasing electron-withdrawing effect of the substituent. Interestingly, the second-order rate constant obtained for the NO₂-substituted catalyst is significantly higher than expected from the trend seen with the other five catalysts. For [MoO₂(L^{NO₂})MeOH], the faster rate of the oxidative half reaction leads to a color change of the solution from yellow/orange to orange/brown at high conversion, presumably due to the resulting reduced Mo-species accumulating. It is conceivable that either the oxidative and reductive half-reactions begin to compete in terms of kinetics, or the dissociation of the oxidized product OPPh₃ from the catalyst becomes rate limiting. Absorption spectroscopic studies are underway to investigate these mechanistic aspects further.

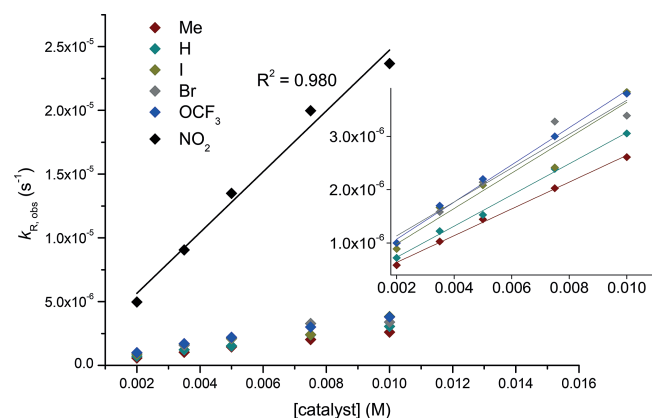


Figure 8. Linear relationships between k_{obs} and catalyst concentrations used for the determination of the second-order rate constants k_2 . The inset shows an expansion of the plots with smaller rate constants.

Summary and Conclusions

From an analysis of the crystal structures, IR and NMR spectroscopic data of six *cis*-dioxo Mo^{VI} complexes with thiosemicarbazone ligands that are derived from *para*-substituted salicylaldehydes, it is evident that the substituents in the *para*-position of the phenolate donor significantly affect the Mo^{VI} ligand interactions and that linear relationships exist between the Hammett constants and key properties of the complexes.

In addition, it was found that EWGs and EDGs have opposite effects on the rate of the oxygen atom transfer from dimethyl sulfoxide to triphenylphosphine. EWGs reduce the electron density on the O and N donor atoms of the ligand and hence the *cis*-dioxomolybdenum core, thereby facilitating a nucleophilic attack by the phosphine substrate. Hence, the reactivity of the *cis*-dioxomolybdenum unit in thiosemicarbazone complexes can be fine-tuned through ligand design, with electron-withdrawing substituents enhancing catalytic OAT activity.

Experimental Section

Materials and Instrumentation: 2-Hydroxy-5-nitrobenzaldehyde, 2-hydroxy-5-methylbenzaldehyde, 2-hydroxy-5-(trifluoromethoxy)benzaldehyde, 5-iodosalicylaldehyde, 4-ethyl-3-thiosemicarbazide, triphenylphosphine, sodium molybdate dihydrate, deuterated dichloromethane and DMSO were purchased from Aldrich. Salicylaldehyde was purchased from Fluka, 2-hydroxy-5-bromobenzaldehyde from Alfa Aesar, acetylacetone from BDH Chemicals. Solvents for syntheses were dried and stored over 3 Å molecular sieves. [MoO₂(acac)₂] was synthesized according to a reported procedure.^[46] Triphenylphosphine was recrystallized from hot ethanol prior to use. ¹H and ¹³C{¹H} decoupled NMR spectra were recorded with a Jeol ECS400 instrument (¹H NMR 400 MHz, ¹³C NMR 100.6 MHz). Assignment of resonances was confirmed by COSY, DEPT135 and HSQC spectra. ³¹P{¹H} decoupled NMR spectra for kinetic studies were recorded with a Bruker 500 instrument (¹H NMR 500 MHz, ³¹P NMR 202.4 MHz). IR spectra were recorded in KBr with a Thermo Nicolet Avatar 370 FTIR spectrophotometer in the region of 4000–400 cm⁻¹. Melting points were measured with a Stuart Scientific SMP3 apparatus. Elemental analyses of compounds were carried out with an Exeter CE-440 elemental analyzer. Electron spray ionization mass spectrometry (ESI-MS) and high-resolution mass spectra were recorded with a Bruker microTOF electrospray mass spectrometer. LIFDI measurements were carried out with a Waters GCT Premier orthogonal time-of-flight mass spectrometer equipped with a LIFDI probe from Linden GmbH. Crystallographic data were collected with an Agilent SuperNova diffractometer with Mo- K_{α} radiation ($\lambda = 0.71073 \text{ \AA}$) by using a EOS CCD camera. The crystals were cooled with an Oxford Instruments Cryojet. Face-indexed absorption corrections were applied by using SCALE3 ABSPACK scaling. OLEX2^[47] was used for overall structure solution, refinement and preparation of computer graphics and publication data. Within OLEX2, the algorithms used for structure solution were direct methods using SHELXS-97 and refinement by full-matrix least-squares used SHELXL-97 within OLEX2. All non-hydrogen atoms were refined anisotropically. Hydrogen atoms were placed by using a riding model and included in the refinement at calculated positions, except for acidic hydrogen atoms, which were placed by using

the difference map method. The CCDC numbers given in Table 2 contain the supplementary crystallographic data for this paper. These data can be obtained free of charge from The Cambridge Crystallographic Data Centre via www.ccdc.cam.ac.uk/data_request/cif.

General Procedure for the Synthesis of Thiosemicarbazones: A solution of 4-ethyl-3-thiosemicarbazide (3.36 mmol) and the appropriate 5-substituted-2-hydroxybenzaldehyde (3.36 mmol) in ethanol (40 mL) was heated to reflux overnight. After cooling to room temperature, the solvent was partially evaporated and, once the product started to precipitate, the mixture was cooled in an ice bath. The product was collected by filtration, washed with cold ethanol and dried.

H₂L^H: Yield 56%; m.p. 165–166 °C. ¹H NMR (400 MHz, [D₆]-DMSO, 25 °C): δ = 11.37 (s, 1 H, NH), 9.91 (s, 1 H, OH), 8.47 (t, ³J_{H,H} = 5.88 Hz, 1 H, NH), 8.36 (s, 1 H, CH), 7.94 (d, ³J_{H,H} = 7.8 Hz, 1 H, CH_{Ar}), 7.21 (t, ³J_{H,H} = 7.72 Hz, 1 H, CH_{Ar}), 6.86 (d, ³J_{H,H} = 8.28 Hz, 1 H, CH_{Ar}), 6.83 (t, ³J_{H,H} = 7.68 Hz, 1 H, CH_{Ar}), 3.58 (m, 2 H, CH₂), 1.14 (t, ³J_{H,H} = 7.12 Hz, 3 H, CH₃) ppm. ¹³C NMR (100 MHz, [D₆]-DMSO, 25 °C): δ = 176.5, 156.4, 139.0, 131.0, 126.6, 120.5, 119.2, 116.1, 38.3, 14.7 ppm. MS-ESI: *m/z* calcd. [M + H⁺] 224.0852; found 224.0848; *m/z* calcd. [M + Na⁺] 246.0672; found 246.0661. C₁₀H₁₃N₃OS (223.29): C 53.79, H 5.87, N 18.82; found C 53.80, H 5.86, N 18.83.

H₂L^{Me}:^[29] Yield 46%; m.p. 168–169 °C. ¹H NMR (400 MHz, [D₆]-DMSO, 25 °C): δ = 11.33 (s, 1 H, NH), 9.65 (s, 1 H, OH), 8.44 (t, ³J_{H,H} = 5.9 Hz, 1 H, NH), 8.33 (s, 1 H, CH), 7.71 (d, ⁴J_{H,H} = 1.8 Hz, 1 H, CH_{Ar}), 7.02 (dd, ³J_{H,H} = 8.3, ⁴J_{H,H} = 2.3 Hz, 1 H, CH_{Ar}), 6.76 (d, ³J_{H,H} = 8.2 Hz, 1 H, CH_{Ar}), 3.59 (m, ³J_{H,H} = 7.1 Hz, 2 H, CH₂), 2.23 (s, 3 H, CH₃), 1.14 (t, ³J_{H,H} = 7.1 Hz, 3 H, CH₃) ppm. ¹³C NMR (100 MHz, [D₆]-DMSO, 25 °C): δ = 176.4, 154.3, 139.4, 131.7, 127.8, 126.5, 120.0, 115.9, 38.3, 20.2, 14.7 ppm. MS-ESI: *m/z* calcd. [M + H⁺] 238.1009; found 238.1005; *m/z* calcd. [M + Na⁺] 260.0828; found 260.0818. C₁₁H₁₅N₃OS (237.32): calcd. C 55.67, H 6.37, N 17.71; found C 55.73, H 6.34, N 17.77. The melting point and NMR resonances are consistent with those previously reported.^[29]

H₂L^{Br}:^[34] Yield 39%; m.p. 200–201 °C. ¹H NMR (400 MHz, [D₆]-DMSO, 25 °C): δ = 11.42 (s, 1 H, NH), 10.26 (s, 1 H, OH), 8.65 (t, ³J_{H,H} = 5.9 Hz, 1 H, NH), 8.29 (s, 1 H, CH), 8.16 (d, ⁴J_{H,H} = 2.6 Hz, 1 H, CH_{Ar}), 7.34 (dd, ³J_{H,H} = 8.7, ⁴J_{H,H} = 2.6 Hz, 1 H, CH_{Ar}), 6.82 (d, ³J_{H,H} = 8.7 Hz, 1 H, CH_{Ar}), 3.59 (dq, ³J_{H,H} = 7.0 Hz, 2 H, CH₂), 1.14 (t, ³J_{H,H} = 7.1 Hz, 3 H, CH₃) ppm. ¹³C NMR (100 MHz, [D₆]-DMSO, 25 °C): δ = 176.6, 155.6, 136.9, 133.2, 128.1, 123.0, 118.2, 111.0, 38.3, 14.7 ppm. MS-ESI: *m/z* calcd. [M + H⁺] 301.9957; found 301.9948; *m/z* calcd. [M + Na⁺] 323.9777; found 323.9766. C₁₀H₁₂BrN₃OS (302.19): calcd. C 39.75, H 4.00, N 13.91; found C 39.99, H 4.05, N 13.81. The melting point and NMR resonances are consistent with those previously reported.^[34]

H₂L^I: Yield 68%; m.p. 221–222 °C. ¹H NMR (400 MHz, [D₆]-DMSO, 25 °C): δ = 11.39 (s, 1 H, NH), 10.22 (s, 1 H, OH), 8.61 (t, ³J_{H,H} = 5.92 Hz, 1 H, NH), 8.27 (s, 1 H, CH), 8.24 (d, ⁴J_{H,H} = 2.28 Hz, 1 H, CH_{Ar}), 7.49 (dd, ³J_{H,H} = 8.6, ⁴J_{H,H} = 2.28 Hz, 1 H, CH_{Ar}), 6.70 (d, ³J_{H,H} = 8.6 Hz, 1 H, CH_{Ar}), 3.59 (m, ³J_{H,H} = 7.04 Hz, 2 H, CH₂), 1.15 (t, ³J_{H,H} = 7.08 Hz, 3 H, CH₃) ppm. ¹³C NMR (100 MHz, [D₆]-DMSO, 25 °C): δ = 177.0, 156.6, 139.6, 137.6, 134.3, 123.9, 119.1, 82.5, 38.7, 15.2 ppm. MS-ESI: *m/z* calcd. [M + H⁺] 349.9819; found 349.9829; *m/z* calcd. [M + Na⁺]

371.9638; found 371.9637. C₁₀H₁₂N₃OIS: calcd. C 34.40, H 3.46, N 12.03; found C 34.48, H 3.42, N 11.85.

H₂L^{OCF₃}: Yield 48%; m.p. 161–162 °C. ¹H NMR (400 MHz, [D₆]-DMSO, 25 °C): δ = 11.41 (s, 1 H, NH), 10.33 (s, 1 H, OH), 8.60 (t, ³J_{H,H} = 6.0 Hz, 1 H, NH), 8.28 (s, 1 H, CH), 7.96 (d, ⁴J_{H,H} = 3.2 Hz, 1 H, CH_{Ar}), 7.16 (m, 1 H, CH_{Ar}), 6.89 (d, ³J_{H,H} = 9.2 Hz, 1 H, CH_{Ar}), 3.55 (quin, ³J_{H,H} = 6.9 Hz, 2 H, CH₂), 1.1 (t, ³J_{H,H} = 7.1 Hz, 3 H, CH₃) ppm. ¹³C NMR (100 MHz, [D₆]-DMSO, 25 °C): δ = 177.1, 155.8, 141.5, 137.5, 124.0, 122.4, 119.4, 117.7, 38.8, 15.2 ppm. MS-ESI: *m/z* calcd. [M + H⁺] 308.0675; found 308.0666; *m/z* calcd. [M + Na⁺] 330.0495; found 330.0481. C₁₁H₁₂F₃N₃O₂S + 0.4 CH₃OH: calcd. C 42.77, H 4.28, N 13.13; found C 42.40, H 3.90, N 13.50.

H₂L^{NO₂}: Yield 95%; m.p. 201–202 °C. ¹H NMR (400 MHz, [D₆]-DMSO, 25 °C): δ = 11.57 (s, 1 H, OH), 11.52 (s, 1 H, NH), 8.81 (d, ⁴J_{H,H} = 2.9 Hz, 1 H, CH_{Ar}), 8.75 (t, ³J_{H,H} = 6.0 Hz, NH), 8.37 (s, 1 H, CH), 8.11 (dd, ³J_{H,H} = 9.1, ⁴J_{H,H} = 2.9 Hz, 1 H, CH_{Ar}), 7.05 (d, ³J_{H,H} = 9.1 Hz, CH_{Ar}), 3.60 (m, ³J_{H,H} = 7.0 Hz, CH₂), 1.15 (t, ³J_{H,H} = 7.1 Hz, CH₃) ppm. ¹³C NMR (100 MHz, [D₆]-DMSO, 25 °C): δ = 176.7, 161.9, 140.3, 136.4, 126.3, 122.0, 121.5, 116.5, 38.3, 14.6 ppm. MS-ESI: *m/z* calcd. [M + H⁺] 269.0703; found 269.0705; *m/z* calcd. [M + Na⁺] 291.0522; found 291.0525. C₁₀H₁₂N₄O₃S₁ + 0.55H₂O + 0.45CH₃OH: calcd. C, 42.89, H, 5.13, N, 19.15; found C, 43.11, H, 4.72, N, 18.75.

General Procedure for the Synthesis of [MoO₂(L)MeOH]: A solution of [MoO₂(acac)₂] (0.2 g, 0.61 mmol) and the appropriate thiosemicarbazone ligand (0.61 mmol) in methanol (30 mL) was heated to reflux overnight. After cooling to room temperature, the mixture was concentrated until the product started to precipitate, then the flask was cooled in an ice bath. The precipitated product was collected by filtration, washed with cold methanol, and dried under vacuum.

[MoO₂(L^H)MeOH]: Yield 46%; m.p. 120–121 °C (dec.). ¹H NMR (400 MHz, [D₆]-DMSO, 25 °C): δ = 8.55 (s, 1 H, CH), 7.60 (dd, ³J = 7.76, ⁴J = 1.68 Hz, 1 H, CH_{Ar}), 7.52 (t, ³J = 5.12 Hz, 1 H, NH), 7.40 (ddd, ³J = 9, ³J = 7.24, ⁴J = 1.72 Hz, 1 H, CH_{Ar}), 6.98 (ddd, ³J = 7.72, ⁴J = 1.12 Hz, 1 H, CH_{Ar}), 6.85 (d, ³J = 8.28 Hz, 1 H, CH_{Ar}), 4.11 (q, 1 H, OH), 3.27 (qd, ³J = 7.20, ³J = 5.36 Hz, 2 H, CH₂), 3.16 (d, 3 H, CH₃), 1.12 (t, ³J = 7.20 Hz, 3 H, CH₃) ppm. ¹³C NMR (100 MHz, [D₆]-DMSO, 25 °C): δ = 158.6, 151.4, 133.4, 133.2, 121.1, 120.7, 117.9, 101.5, 48.6, 38.8, 14.5 ppm. MS-LIFDI: *m/z* calcd. for ⁹⁸Mo [M⁺ – MeOH] 350.9575; found 350.9574. IR (KBr): $\tilde{\nu}$ = 3365 (s), 2977, 1598 (s), 1555 (s), 1516 (s), 1476, 1438, 1288, 930 (s, $\nu_{\text{Mo=O}}$), 901 (s, $\nu_{\text{Mo=O}}$), 726 (s) cm⁻¹. C₁₁H₁₅MoN₃O₄S: calcd. C 34.65, H 3.97, N 11.02; found C 34.84, H 3.91, N 10.82.

[MoO₂(L^{Me})MeOH]:^[29] Yield 79%; m.p. 128–129 °C (dec.). ¹H NMR (400 MHz, [D₆]-DMSO, 25 °C): δ = 8.47 (s, 1 H, CH), 7.49 (t, 1 H, NH), 7.38 (d, ⁴J = 1.96 Hz, 1 H, CH_{Ar}), 7.21 (dd, ³J = 8.40, ⁴J = 2.04 Hz, 1 H, CH_{Ar}), 6.75 (d, ³J = 8.36 Hz, 1 H, CH_{Ar}), 4.11 (q, 1 H, OH), 3.27 (qd, ³J = 7.20, ³J = 5.40 Hz, 2 H, CH₂), 3.17 (d, 3 H, CH₃), 2.26 (s, 3 H, CH₃), 1.12 (t, ³J = 7.20 Hz, 3 H, CH₃) ppm. ¹³C NMR (100 MHz, [D₆]-DMSO, 25 °C): δ = 156.8, 151.4, 133.9, 133.1, 129.6, 120.8, 117.6, 48.6, 38.8, 20.0, 14.5 ppm. MS-LIFDI: *m/z* calcd for ⁹⁸Mo [M⁺ – MeOH] 364.9731; found 364.9749. IR (KBr): $\tilde{\nu}$ = 3382 (s), 1560 (s), 1506 (s), 1475, 1286, 1020, 934 (s, $\nu_{\text{Mo=O}}$), 896 (s, $\nu_{\text{Mo=O}}$) cm⁻¹. C₁₂H₁₇MoN₃O₄S: calcd. C 36.46, H 4.33, N 10.63; found C 36.57, H 4.32, N 10.39. The IR spectrum is consistent with that previously reported.^[29]

[MoO₂(L^{Br})MeOH]:^[34] Yield 99%; m.p. 109–110 °C (dec.). ¹H NMR (400 MHz, [D₆]-DMSO, 25 °C): δ = 8.53 (s, 1 H, CH), 7.83

(d, $^4J = 2.6$ Hz, 1 H, CH_{Ar}), 7.65 (s, 1 H, NH), 7.51 (dd, $^3J = 8.76$, $^4J = 2.6$ Hz, 1 H, CH_{Ar}), 6.82 (d, $^3J = 8.92$ Hz, 1 H, CH_{Ar}), 4.11 (q, 1 H, OH), 3.28 (dq, $^3J = 7.24$, $^3J = 5.40$ Hz, 2 H, CH_2), 3.17 (d, 3 H, CH_3), 1.12 (t, $^3J = 7.20$ Hz, 3 H, CH_3) ppm. ^{13}C NMR (100 MHz, $[D_6]DMSO$, 25 °C): $\delta = 157.8$, 149.9, 135.2, 134.9, 123.3, 120.2, 111.5, 48.6, 38.9, 14.4 ppm. MS-LIFDI: m/z calcd for ^{98}Mo , ^{79}Br [$M^{+} - MeOH$] 428.8680; found 428.8651. IR (KBr): $\tilde{\nu} = 3293.64$ (s), 1592 (s), 1549 (s), 1523 (s), 1469 (s), 1328, 1266, 942 (s, $\nu_{Mo=O}$), 906 (s, $\nu_{Mo=O}$), 818 cm^{-1} . $C_{11}H_{14}BrMoN_3O_4S + 0.85CH_3OH$: calcd. C 29.20, H 3.60, N 8.62; found C 29.06, H 3.44, N 8.48. The IR data and NMR resonances are consistent with those previously reported.^[34]

[MoO₂(L¹)MeOH]: Yield 42%; m.p. 116–117 °C (dec.). 1H NMR (400 MHz, $[D_6]DMSO$, 25 °C): $\delta = 8.50$ (s, 1 H, CH), 7.96 (d, $^4J = 2.28$ Hz, 1 H, CH_{Ar}), 7.64 (s, 1 H, NH), 7.64 (dd, $^3J = 8.64$, $^4J = 2.28$ Hz, 1 H, CH_{Ar}), 6.68 (d, $^3J = 8.6$ Hz, 1 H, CH_{Ar}), 3.27 (dq, $^3J_1 = 7.20$, $^3J_2 = 5.40$ Hz, 2 H, CH_2), 3.16 (s, 3 H, CH_3), 1.12 (t, $^3J = 7.20$ Hz, 3 H, CH_3) ppm. ^{13}C NMR (100 MHz, $[D_6]DMSO$, 25 °C): $\delta = 158.3$, 149.8, 140.9, 140.8, 123.9, 120.5, 82.6, 48.6, 38.9, 14.4 ppm. MS-LIFDI: m/z calcd. for ^{98}Mo [$M^{+} - MeOH$] 476.85; found 476.85. IR (KBr): $\tilde{\nu} = 3297$ (s), 1589 (s), 1543 (s), 1519, 1467, 937 (s, $\nu_{Mo=O}$), 906 (s, $\nu_{Mo=O}$) cm^{-1} . $C_{11}H_{14}N_3O_4SMo + 0.5CH_3OH$: calcd. C 26.40, H 3.08, N 8.03; found C 26.13, H 3.14, N 7.52.

[MoO₂(L^{OCF₃)MeOH]:} Yield 35%; m.p. 108–109 °C (dec.). 1H NMR (400 MHz, $[D_6]DMSO$, 25 °C): $\delta = 7.81$ (s, 1 H, CH), 6.92 (d, $^4J = 2.7$ Hz, 1 H, CH_{Ar}), 6.60 (dd, $^3J = 8.70$, $^4J = 2.70$ Hz, 1 H, CH_{Ar}), 6.17 (d, $^3J = 8.70$ Hz, 1 H, CH_{Ar}), 3.33 (br. s, NH), 1.73 (m, CH_2), 0.34 (t, $^3J = 7.10$ Hz, 3 H, CH_3) ppm. ^{13}C NMR (100 MHz, $[D_6]DMSO$, 25 °C): $\delta = 157.5$, 150.0, 141.2, 125.9, 125.3, 122.0, 119.52, 119.0, 48.7, 38.8, 14.48 ppm. MS-LIFDI: m/z calcd. for ^{98}Mo [$M^{+} - MeOH$] 434.97; found 434.94. IR (KBr): $\tilde{\nu} = 3390$, 1557, 1518, 1257 (s), 1214 (s), 1155, 937 (s, $\nu_{Mo=O}$), 908.5 (s, $\nu_{Mo=O}$) cm^{-1} . $C_{12}H_{14}N_3O_5F_3SMo$: calcd. C 30.98, H 3.03, N 9.03; found C 30.69, H 3.04, N 8.95.

[MoO₂(L^{NO₂)MeOH]:} Yield 40%; m.p. 135–136 °C (dec.). 1H NMR (400 MHz, $[D_6]DMSO$, 25 °C): $\delta = 8.73$ (s, 1 H, CH), 8.64 (d, $^4J = 2.88$ Hz, 1 H, CH_{Ar}), 8.21 (dd, $^3J = 9.08$, $^4J = 2.92$ Hz, 1 H, CH_{Ar}), 7.80 (s, 1 H, NH), 7.03 (d, $^3J = 9.12$ Hz, 1 H, CH_{Ar}), 4.11 (q, 1 H, OH), 3.30 (m, 2 H, CH_2), 3.16 (d, 3 H, CH_3), 1.14 (t, $^3J = 7.20$ Hz, 3 H, CH_3) ppm. ^{13}C NMR (100 MHz, $[D_6]DMSO$): $\delta = 163.4$, 150.1, 140.3, 129.4, 127.9, 121.5, 119.4, 48.6, 40.6, 14.4 ppm. MS-LIFDI: m/z calcd. for ^{98}Mo [$M^{+} - MeOH$] 395.94; found 395.93. IR (KBr): $\tilde{\nu} = 3321$ (s), 1600 (s), 1559, 1511 (s), 1475, 1339 (s), 1297 (s), 941 (s, $\nu_{Mo=O}$), 899 (s, $\nu_{Mo=O}$) cm^{-1} . $C_{11}H_{14}N_4O_6SMo + 0.75H_2O$: calcd. C 30.04, H 3.55, N 12.74; found C 29.80, H 3.29, N 12.53.

Kinetic Studies: Samples were prepared from a solution of Ph_3P in CD_2Cl_2 (255 mM, solution A) and a solution of the respective molybdenum complex in $[D_6]DMSO$ at a known concentration (solution B). 0.4 mL of solution B was added to 0.4 mL of solution A. A color change was noted after a few minutes in the case of $[MoO_2(L^{NO_2})MeOH]$ to orange/brown, while the other solutions remained yellow/orange. The Ph_3P conversion into Ph_3PO was followed over time by ^{31}P NMR spectroscopy for each complex at concentrations of 2, 3.5, 5, 7.5, and 10 mM [Equations (1) and (2)]. The conversion rate was determined by integrating the signal at around –6 ppm, attributed to Ph_3P and at around 26 ppm, attributed to Ph_3PO . Pseudo-first-order rate constants k_{obs} were determined by using Equation (3), where $[Ph_3P]$ is the concentration of Ph_3P at time t and $[Ph_3P]_0$ is the initial concentration of Ph_3P . Sec-

ond-order rate constants k_2 were obtained from the slope of the linear plot of k_{obs} vs. catalyst concentration.

$$\text{rate} = k_2 [\text{cat}][Ph_3P] \quad (1)$$

$$\text{rate} = k_{obs}[Ph_3P] \quad (2)$$

$$\ln([Ph_3P]_t/[Ph_3P]_0) = -k_{obs}t \quad (3)$$

Acknowledgments

The authors thank the Engineering and Physical Sciences Research Council (EPSRC) (EP/J019666/1), COST Action (CM1003; “Biological oxidation reactions - mechanisms and design of new catalysts”) and the University of York, UK for financial support. Dr. R. E. Douthwaite is thanked for helpful discussions. Experimental support provided by K. Heaton (mass spectrometry), Dr. A. C. Whitwood and N. Pridmore (X-ray crystallography) is gratefully acknowledged.

- [1] R. Hille, *Chem. Rev.* **1996**, *96*, 2757–2816.
- [2] R. H. Holm, *Chem. Rev.* **1987**, *87*, 1401–1449.
- [3] J. H. Enemark, J. J. A. Cooney, J.-J. Wang, R. H. Holm, *Chem. Rev.* **2004**, *104*, 1175–1200.
- [4] H. Sugimoto, H. Tsukube, *Chem. Soc. Rev.* **2008**, *37*, 2609–2619.
- [5] C. Schulzke, *Eur. J. Inorg. Chem.* **2011**, 1189–1199.
- [6] A. Majumdar, S. Sarkar, *Coord. Chem. Rev.* **2011**, *255*, 1039–1054.
- [7] J.-J. Wang, O. P. Kryatova, E. V. Rybak-Akimova, R. H. Holm, *Inorg. Chem.* **2004**, *43*, 8092–8101.
- [8] A. L. Whalley, A. J. Blake, D. Collison, E. S. Davies, H. J. Disley, M. Helliwell, F. E. Mabbs, J. McMaster, C. Wilson, C. D. Garner, *Dalton Trans.* **2011**, *40*, 10457–10472.
- [9] B. E. Schultz, S. f. Gheller, M. C. Muettterties, M. J. Scott, R. H. Holm, *J. Am. Chem. Soc.* **1993**, *115*, 2714–2722.
- [10] K. Hüttinger, C. Förster, T. Bund, D. Hinderberger, K. Heinze, *Inorg. Chem.* **2012**, *51*, 4180–4192.
- [11] J. Leppin, C. Förster, K. Heinze, *Inorg. Chem.* **2014**, *53*, 12416–12427.
- [12] G. Lyashenko, R. Herbst-Irmer, V. Jancik, A. Pal, N. C. Mösch-Zanetti, *Inorg. Chem.* **2008**, *47*, 113–120.
- [13] M. Volpe, N. C. Mösch-Zanetti, *Inorg. Chem.* **2012**, *51*, 1440–1449.
- [14] C. Doonan, D. J. Nielsen, P. D. Smith, J. M. White, G. N. George, C. G. Young, *J. Am. Chem. Soc.* **2006**, *128*, 305–316.
- [15] P. Basu, V. N. Nemykin, R. S. Sengar, *Inorg. Chem.* **2009**, *48*, 6303–6313.
- [16] P. Basu, B. W. Kail, A. K. Adams, V. N. Nemykin, *Dalton Trans.* **2013**, *42*, 3071–3081.
- [17] J. Topich, J. T. Lyon III, *Polyhedron* **1984**, *3*, 61–65.
- [18] D. Eierhoff, W. C. Tung, A. Hammerschmidt, B. Krebs, *Acta Chim.* **2008**, *362*, 915–928.
- [19] A. Rezaeifard, I. Sheikhshoae, N. Monadi, H. Stoeckli-Evans, *Eur. J. Inorg. Chem.* **2010**, 799–806.
- [20] A. Thapper, A. Behrens, J. Fryxellius, M. H. Johansson, F. Prestopino, M. Czaun, D. Rehder, E. Nordlander, *Dalton Trans.* **2005**, 3566–3571.
- [21] C. J. Whiteoak, G. J. P. Britovsek, V. C. Gibson, A. J. P. White, *Dalton Trans.* **2009**, 2337–2344.
- [22] A. Lehtonen, R. Sillanpää, *Polyhedron* **2005**, *24*, 257–265.
- [23] A. Majumdar, S. Sarkar, *Coord. Chem. Rev.* **2011**, *255*, 1039–1054.
- [24] T. S. Lobana, R. Sharma, G. Bava, S. Khanna, *Coord. Chem. Rev.* **2009**, *253*, 977–1055.
- [25] L. Stelzig, S. Kötte, B. Krebs, *J. Chem. Soc., Dalton Trans.* **1998**, 2921–2926.
- [26] J. Pisk, B. Prugovečki, D. Matković-Čalogović, R. Poli, D. Augustin, V. Vrdoljak, *Polyhedron* **2012**, *33*, 441–449.

- [27] M. Leigh, C. E. Castillo, D. J. Raines, A.-K. Duhme-Klair, *ChemMedChem* **2011**, *6*, 612–616.
- [28] M. Leigh, C. E. Castillo, D. J. Raines, A.-K. Duhme-Klair, *ChemMedChem* **2011**, *6*, 1107–1118.
- [29] M. A. Hussein, T. S. Guan, R. A. Haque, M. B. K. Ahamed, A. M. S. A. Majid, *Inorg. Chim. Acta* **2014**, *421*, 270.
- [30] M. A. Hussein, T. S. Guan, R. A. Haque, M. B. K. Ahamed, A. M. S. A. Majid, *J. Coord. Chem.* **2014**, *67*, 714.
- [31] C. Hansch, A. Leo, R. W. Taft, *Chem. Rev.* **1991**, *91*, 165–195.
- [32] F. Leroux, B. Manteau, J.-P. Vors, S. Pazsnok, *Beilstein J. Org. Chem.* **2008**, *4*, 1–15.
- [33] H. B. Linden, *Eur. J. Mass Spectrom.* **2004**, *10*, 459–468.
- [34] M. A. Hussein, T. S. Guan, R. A. Haque, M. B. K. Ahamed, A. M. S. A. Majid, *Spectrochim. Acta Part A* **2015**, *136*, 1335–1348.
- [35] N. G. Connelly, T. Damhus, R. M. Hartshorn, A. T. Hutton, *Nomenclature of Inorganic Chemistry IUPAC Recommendations*, RSC Publishing, **2005**, IR-9.3.
- [36] The configuration index was assigned based on the Cahn–Ingold–Prelog (CIP) system by using the following priorities: S > O^{Ph} > HO-Me > O^{oxo} > N^{imine}. In octahedral complexes OC-6-*xy*, *x* refers to the ligand *trans* to the ligand of highest priority (axial ligands) and *y* refers to the ligand *trans* to the ligand of highest priority in the equatorial plane. The chirality index reflects the clockwise (C) or anticlockwise (A) sequence of priority numbers of the ligands in the equatorial plane if viewed from the axial atom of highest CIP priority.
- [37] D.-W. Kim, U. Lee, B. K. Koo, *Bull. Korean Chem. Soc.* **2004**, *25*, 1071–1074.
- [38] S. Duman, İ. Kizilcikli, A. Koca, M. Akkurt, B. Ülküseven, *Polyhedron* **2010**, *29*, 2924–2932.
- [39] İ. Kizilcikli, S. Eglence, A. Gelir, *Transition Met. Chem.* **2008**, *33*, 775–779.
- [40] M. A. Hussein, T. S. Guan, R. A. Haque, M. B. K. Ahamed, A. M. S. A. Majid, *Polyhedron* **2015**, *85*, 93–103.
- [41] R. Mayilmurugan, B. N. Harum, M. Volpe, A. F. Sax, M. Palaniandavar, N. C. Mösch-Zanetti, *Chem. Eur. J.* **2011**, *17*, 704–713.
- [42] M. A. Pietsch, M. B. Hall, *Inorg. Chem.* **1996**, *35*, 1273–1278.
- [43] B. W. Kail, L. M. Perez, S. Zaric, A. J. Millar, C. G. Young, M. B. Hall, P. Basu, *Chem. Eur. J.* **2006**, *12*, 7501–7509.
- [44] P. Basu, V. N. Nemykin, R. S. Sengar, *Inorg. Chem.* **2009**, *48*, 6303–6313.
- [45] K.-M. Sung, R. H. Holm, *J. Am. Chem. Soc.* **2002**, *124*, 4312–4320.
- [46] H. Gehrke Jr., J. Veal, *Inorg. Chim. Acta* **1969**, 623–627.
- [47] O. V. Dolomanov, L. J. Bourhis, R. J. Gildea, J. A. K. Howard, H. Puschmann, *J. Appl. Crystallogr.* **2009**, *42*, 339.

Received: January 21, 2015

Published Online: ■

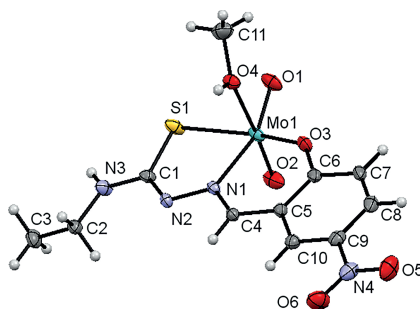
Oxygen Atom Transfer

A. Ducrot, B. Scattergood, B. Coulson,
R. N. Perutz,
A.-K. Duhme-Klair* 1–11



Electronic Fine-Tuning of Oxygen Atom Transfer Reactivity of *cis*-Dioxomolybdenum(VI) Complexes with Thiosemicarbazone Ligands

Keywords: Enzyme models / Metalloenzymes / Molybdenum / Oxygen atom transfer / Ligand effects



Thiosemicarbazone ligands (H_2L^R) derived from *para*-substituted salicylaldehydes allow the electronic properties and catalytic activities of *cis*-dioxo Mo^{VI} complexes of composition $[MoO_2(L^R)MeOH]$ to be fine-tuned by electron-donating or electron-withdrawing groups R.